**Atmospheric
Measurement
Techniques
Discussions**

# Long-term validation of total and tropospheric column-averaged CH$_4$ mole fractions obtained by mid-infrared ground-based FTIR spectrometry

E. Sepúlveda[1,2], M. Schneider[2,3], F. Hase[3], O. E. García[2], A. Gomez-Pelaez[2], S. Dohe[3], T. Blumenstock[3], and J. C. Guerra[1]

[1]La Laguna University, Tenerife, Spain
[2]Izaña Atmospheric Research Center, Agencia Estatal de Meteorología (AEMET), Izaña, Spain
[3]Institute for Meteorology and Climate Research (IMK-ASF), Karlsruhe Institute of Technology, Karlsruhe, Germany

Correspondence to: E. Sepúlveda (esepulvedah@aemet.es)

**AMTD**

**Long-term validation of total and tropospheric CH$_4$ mole fractions**

E. Sepúlveda et al.

Title Page

| Abstract | Introduction |
| Conclusions | References |
| Tables | Figures |

|◄ | ►|

◄ | ►

Back | Close

Full Screen / Esc

Printer-friendly Version

Interactive Discussion

E. Sepúlveda et al.

# Abstract

At the Izaña Atmospheric Research Center high-resolution middle infrared solar absorption spectra have been recorded for more than 12 years using Fourier Transform InfraRed (FTIR) spectrometers. We use the spectral fitting algorithm PROFFIT to retrieve long-term time series of methane (CH$_4$) from the measured spectra. We investigate the total column-averaged dry-air mole fractions of methane (totXCH4) obtained from a scaling and a profile retrieval, and apply two approaches for deriving the tropospheric column-averaged dry-air mole fractions: firstly, we use the FTIR Hydrogen Fluoride (HF) total column amounts as an estimator for the stratospheric CH$_4$ contribution and a posteriori correct the totXCH4 data of a profile scaling retrieval accordingly (troXCH4$_{post}$), and secondly, we directly determine the tropospheric column-averaged dry-air mole fractions of methane (troXCH4$_{retr}$) from retrieved CH$_4$ profiles. Our theoretical estimation indicates that the scaling retrieval leads to totXCH4 amounts that are subject to a large smoothing error, which can be widely avoided by applying a profile retrieval (for the latter we estimate an overall precision of 0.41 %).

We compare the different FTIR CH$_4$ data to Izaña's Global Atmospheric Watch (GAW) surface in-situ CH$_4$ data (CH$_{4_{GAW}}$), which in the case of the Izaña Atmospheric Research Center high mountain observatory are well representative for the free tropospheric CH$_4$ amounts. Concerning totXCH4 the agreement between the FTIR data product and the in-situ measurement is rather poor documenting that totXCH4 is no valid free tropospheric CH$_4$ proxy instead it is significantly affected by the varying stratospheric CH$_4$ contribution and it rather follows the variation in the tropopause altitude. The a posteriori correction method only removes a part of this stratospheric CH$_4$ contribution. On the contrary the profile retrieval allows for a direct estimation of the tropospheric column-averaged CH$_4$ amounts. This troXCH4$_{retr}$ data correlates well with the CH$_{4_{GAW}}$ data (correlation coefficient of 0.60, FTIR-GAW scatter of 0.97 %) and both data show very similar annual cycles and trend behaviour (for the 2001–2010 time period). Furthermore, we find a very good absolute agreement between the troXCH4$_{retr}$

and $CH_{4_{GAW}}$ (middle infrared FTIR/GAW scaling factor of 0.9987) suggesting that middle infrared FTIR data can be well combined with the surface in-situ GAW data.

Our study proves the significance of middle infrared ground-based FTIR $CH_4$ profile retrievals as well as the robustness of the approach for achieving total and tropospheric
5  column-averaged $X CH_4$ data of high quality.

# 1  Introduction

Methane ($CH_4$) is the second most important anthropogenic greenhouse gas (GHG), after carbon dioxide ($CO_2$). While $CH_4$ is 200 times less abundant than $CO_2$, it is about 20 times more efficient than $CO_2$ to trap outgoing long wave radiation, on a 50 years
10  timescale. The change in the $CH_4$ mixing ratio since pre-industrial times (1750) to 2005 (from 715 to 1774 ppb) gives a radiative forcing (RF) of $+0.48 \pm 0.05\,W\,m^{-2}$, ranking $CH_4$ as the second highest RF of the GHGs after $CO_2$ (RF of $CO_2$ in 2005, $1.66 \pm 0.17\,W\,m^{-2}$; IPCC, 2007). In 2009 $CH_4$ global atmospheric concentrations have reached more than 1780 ppb for column-averaged mole fractions on global average in
15  2009 (Frankenberg et al., 2011). At surface stations higher annual average values are registered (e.g. 1830 ppb at the Izaña's Global Atmospheric Watch, GAW, station in 2009, Gomez-Pelaez, 2010).

$CH_4$ plays an important role in atmospheric chemistry, affecting the oxidizing capacity of the atmosphere and acting as a precursor of tropospheric ozone ($O_3$). The main
20  sources producing methane are considered to be: Biogenic $CH_4$ formation that occurs in natural wetlands, water-flooded rice paddies, landfills and stomachs of ruminant animals, incomplete burning of biomass, oceans and vegetation. Further sources are release from melting permafrost and from shallow hydrates on the continental shelf (Dlugokencky et al., 2009). Thermogenic formation is the main process for generation
25  of natural gas deposits over geological time scales, parts of this inventory is released into the atmosphere due to fossil fuel extraction, processing, transportation and distribution (Keppler et al., 2006; Frankenberg et al., 2005). The main sink of atmospheric

**Long-term validation of total and tropospheric CH$_4$ mole fractions**

E. Sepúlveda et al.

CH$_4$ is the reaction with hydroxyl radical (OH). The destruction of CH$_4$ by OH in the troposphere represents about 90 % of CH$_4$ loss in the atmosphere. The rest of the sink is due to an uptake of CH$_4$ by soils, reaction with Cl in the marine boundary layer, and due to transport into the stratosphere where it is decomposed by reactions with OH, O($^1$D) and Cl (Bousquet et al., 2011).

Prediction of the evolution of GHGs in the atmosphere requires an understanding of their sources and sinks. Therefore, inverse modelling techniques applying atmospheric concentration measurement monitored at global surface networks are used (Bousquet et al., 2011). The in-situ surface measurements show very high-precision and absolute accuracy (approx. 0.1 %), but they are strongly affected by local processes like small scale turbulences or nearby sources or sinks. It is very difficult for the inverse models to capture these small scale processes. In this context vertically averaging the concentrations can be helpful. For instance, Olsen and Randerson (2004) document that total column averaged observations of GHGs are significantly less affected by small scale processes, but still conserve valuable GHG source/sink information. However, total column-averaged data are affected by the stratospheric contribution, the correct modelling of which is a significant error source when investigating the GHG cycling between the atmosphere, the biosphere, and the ocean.

Ground-based high spectral resolution FTIR measurements allow a precise determination of the atmospheric abundances (total column amounts and vertical profiles) of many constituents, including GHGs. The ground-based FTIR total column data are essential for the validation of GHGs measured from space by current and future satellite sensors: (e.g. SCIAMACHY, GOSAT, OCO-2). Furthermore, by means of the ground-based FTIR vertical profile data one can calculate tropospheric column averaged mixing ratios. These ratios would not be affected by small scale surface near processes neither by stratospheric contributions. If provided with high accuracy and precision, the tropospheric column averaged mixing ratios would be a very useful data product for investigating the GHG cycling between the atmosphere, the biosphere, and the ocean.

**Long-term validation of total and tropospheric CH$_4$ mole fractions**

E. Sepúlveda et al.

Title Page

| Abstract | Introduction |
| Conclusions | References |
| Tables | Figures |

◀ | ▶

◀ | ▶

Back | Close

Full Screen / Esc

Printer-friendly Version

Interactive Discussion

**Long-term validation of total and tropospheric CH$_4$ mole fractions**

E. Sepúlveda et al.

In this work we present, discuss, and validate different ground-based FTIR CH$_4$ products: the total column-averaged volume mixing ratio (totXCH$_4$), and two tropospheric column averaged volume mixing ratios (troXCH$_4$): a first derived by a posteriori correction method using HF as indicator for the stratospheric contribution (similar to Washenfelder et al., 2003), and a second directly retrieved from the measured spectra.

In the following Sect. 2 we describe the CH$_4$ program at the Izaña Atmospheric Research Center: the GAW in-situ and FTIR activities. In Sect. 3 we present the FTIR technique and the FTIR CH$_4$ products. We describe the data analysis method and document the characteristics of the FTIR data (sensitivity and uncertainty). In Sect. 4 the different FTIR CH$_4$ products are compared to the GAW surface CH$_4$ measurements and Sect. 5 summarizes our study.

## 2  CH$_4$ program at the Izaña Atmospheric Research Center

### 2.1  Site description

Izaña is a subtropical high mountain observatory located on the Canary Island of Tenerife, 300 km from the African west coast at 28°18′ N, 16°29′ W at 2370 m a.s.l. It is part of the Meteorological State Agency of Spain (Spanish acronym: AEMET) and it is run by the Izaña Atmospheric Research Center. It is a global station of the WMO (World Meteorological Organisation) network of GAW (Global Atmospheric Watch) stations and has a comprehensive measurement program of a large variety of different atmospheric constituents. More detailed information can be found in the official webpage of the Izaña Atmospheric Research Center: http://www.izana.org.

The Izaña Observatory is usually located above a strong subtropical temperature inversion layer (generally well established between 500 and 1500 m a.s.l.). While during daytime the strong diurnal insolation generates a slight upslope flow of air originated from below the inversion layer (from a wood that surrounds the station at a lower

altitude), during night-time the Izaña Observatory is well representative of the free tro-
posphere (or at least of the lower levels of the free troposphere, see Fig. 1).

## 2.2 In-situ measurement program

Continuous surface in-situ measurements of atmospheric $CO_2$ and $CH_4$ have been
carried out at Izaña station since 1984. Furthermore, CO concentrations have been
measured since 1998 and $N_2O$ and $SF_6$ since 2007.

$CH_4$ mole fraction is measured using a DANI 3800 gas chromatograph. The carrier
gas is synthetic air. Ambient air is cooled to −70 °C to partially remove water vapour
content before flowing towards the sample loop (10 ml size). Sample loop temperature
is not regulated. A self-developed software integrator provides the area and height
of the $CH_4$ peak in the chromatogram. See Gomez-Pelaez et al. (2011), and refer-
ences therein, for more details about the measurements and technique. The most
recent World Calibration Centre (WCC-Empa) system and performance audit for $CH_4$
at Izaña was carried in 2009 and documents the good quality of the Izaña $CH_4$ in-situ
data (Zellweger et al., 2009). This good data quality is also confirmed by the contin-
uous comparison to NOAA data obtained from simultaneously collected weekly flask
samples (Gomez-Pelaez et al., 2012).

## 2.3 FTIR measurement program

Ground-based FTIR activities started at Izaña Observatory in the late 1990s in the
framework of a collaboration between AEMET and KIT (Karlsruhe Institute of Tech-
nology, Germany). In 1999 KIT scientists installed a Bruker IFS 120M instrument
at Izaña. In early 2005 KIT substituted this spectrometer by a Bruker IFS 125HR.
During March-April of 2005 both instruments were running side-by-side. The Izaña
FTIR experiment is involved in two global networks: since 1999 it has contributed
to the Network for the Detection of Atmospheric Composition Change (NDACC, http:
//www.ndacc.org) and since 2007 to the Total Carbon Column Observing Network

(TCCON, http://www.tccon.caltech.edu). For NDACC solar absorption spectra are measured in the middle infrared (MIR) spectral region (740–4250 cm$^{-1}$; corresponding to 13.5–2.4 μm) and for TCCON in the near infrared (NIR) spectral region (3500–14 000 cm$^{-1}$; corresponding to 2.9–0.7 μm). The applied high resolution FTIR spectrometer allows for a detailed observation of the pressure broadening effect, i.e. the absorption line width of an atmospheric absorber depends on the pressure (and thus altitude) where the absorption takes place. Therefore, one can retrieve concentration profiles of the atmospheric absorbers in addition to total column abundances. The Instrumental Line Shape (ILS) also affects the observed line shape and in particular for the profile retrievals a continuous monitoring of the ILS is important. At Izaña we determine the ILS about every 2 months by low pressure gas cell (HBr and N$_2$O) measurements and the LINEFIT software (LINEFIT code, Hase et al., 1999). The respective LINEFIT results are then applied in the atmospheric retrievals.

CH$_4$ has absorption lines in both the MIR and NIR spectral regions. In this study we present CH$_4$ retrieved from NDACC MIR spectra.

## 3 Ground-based FTIR technique and CH$_4$ products

### 3.1 General setup of a ground-based FTIR analysis

Ground-based NDACC FTIR systems measure solar absorption spectra, under clear sky conditions, applying a high resolution Fourier Transform Spectrometer (typical resolution of 0.005 cm$^{-1}$; maximum optical path difference, OPD$_{max}$ of 180 cm). The measured spectra are simulated by a precise line-by-line radiative transfer model that applies the parameters of a spectroscopic database (e.g. HITRAN, Rothman et al., 2009). The basic equation for analyzing the solar absorption is the Lambert Beer's law:

$$I(\lambda) = I_{sun}(\lambda) \cdot \exp \left( -\int_{TOA}^{Obs} \sigma_x \left( \lambda, \, s(T, \, p) \right) \cdot x(s) \, ds \right) \tag{1}$$

where $I(\lambda)$ is the measured intensity at wavelength $\lambda$, $I_{sun}$ the extraterrestrial solar intensity, $\sigma_x(\lambda, s)$ is the absorption cross section and x(s) the concentration of an absorber $x$ at location $s$. The integration is performed along the path of the direct sunlight (between the Observer, Obs, and the Top Of the Atmosphere, TOA). At higher wavenumbers (above $1500\,\mathrm{cm}^{-1}$) atmospheric self-emission can be neglected as compared to direct solar radiances.

For the purpose of numerical handling, the atmospheric state x(s) and the simulated spectrum $I(\lambda)$ are discretized in form of a state vector $\boldsymbol{x}$ and a measurement vector $\boldsymbol{y}$. The measurement and state vector are related by a vector valued function $\boldsymbol{F}$ which simulates the atmospheric radiative transfer and the characteristics of the measurement system (spectral resolution, instrumental line shape, etc.): $\boldsymbol{y} = \boldsymbol{F}(\boldsymbol{x})$. The derivatives $\partial\boldsymbol{y}/\partial\boldsymbol{x}$ determine the changes in the modeled spectral fluxes $\boldsymbol{K}$: $\partial\boldsymbol{y} = \boldsymbol{K}\partial\boldsymbol{x}$. Direct inversion of this last equation would allow an iterative calculation of the sought variables $\boldsymbol{x}$. However, the problem is generally ill-determined, i.e. the columns of $\boldsymbol{K}$ are not linearly independent and there are many solutions that are in acceptable agreement with the measurement. Thus, the solution has to be properly constrained. An extensive treatment of this topic is given in the textbook of C. D. Rodgers (Rodgers, 2000). We apply the retrieval code PROFFIT and the included radiative transfer code PROFFWD to accomplish our analysis (Hase et al., 2004).

## 3.2 The CH$_4$ retrieval strategy

Currently the establishment of an improved NDACC CH$_4$ retrieval guideline is under discussion. The objective is an NDACC CH$_4$ product that approaches the high precision requirements of TCCON (a few permil). At some stations NDACC measurements are performed since the early 1990s and high quality NDACC CH$_4$ data could well complement the TCCON time series, which are limited to the last few years.

Our CH$_4$ retrieval strategy is a modification of the current official NDACC retrieval guideline and includes a set of 4 microwindows containing strong, unsaturated, and isolated CH$_4$ lines (see Fig. 2 and Table 1). Besides CH$_4$ we have considered

E. Sepúlveda et al.

spectroscopic signatures of 7 interfering species. For the target species CH$_4$ and the interfering species CO$_2$, O$_3$, N$_2$O, NO$_2$ and HCl we have applied spectroscopic parameters from HITRAN 2008 (Rothman et al., 2009), while for H$_2$O and OCS we have applied the recent HITRAN 2009 update.

As a-priori profiles of the interfering species we apply the climatological entries from WACCM (The Whole Atmosphere Community Climate Model) provided by NCAR (National Centre for Atmospheric Research, J. Hannigan, private communication, 2009). For the minor interfering species (O$_3$, N$_2$O, HCl and OCS) we simply simulate the spectral signatures according to the WCCAM concentrations. For the major absorbers CO$_2$ and NO$_2$ we scale the WCCAM profiles during the CH$_4$ retrieval process and the H$_2$O interferences are accounted for by a two step strategy: first we perform a dedicated H$_2$O retrieval (Schneider et al., 2010a) and then we scale the retrieved daily mean H$_2$O profile in the subsequent CH$_4$ retrieval process. Thereby we minimise the interferences due to H$_2$O and HDO. Such interferences have been investigated in recent studies applying different sets of microwindows. The best strategy to minimize the H$_2$O impact is currently under discussion (Sussmann et al., 2011; Hase et al., 2011). Izaña is a rather dry high-altitude site, so the H$_2$O interference problem is less severe than for low latitude sites at sea-level. We expect that our results are transferable to at least other high altitude or polar sites of the NDACC.

Furthermore, we fit the continuum background slope and the residual ILS asymmetry. We use the NCEP analysis (National Centers for Environmental Prediction) at 12:00 UT as the temperature and pressure input profiles.

We examine two different CH$_4$ fitting procedures. A first consists in scaling the CH$_4$ WACCM a-priori profile (in the following referred to as scaling retrieval, SR) and a second retrieves CH$_4$ profiles (profile retrieval, PR) whereby a Tikhonov-Phillips method on a logarithmic scale is applied (Hase, 2000; Hase et al., 2004; Schneider et al., 2006).

### 3.3 The FTIR CH$_4$ products

#### 3.3.1 Total column-averaged dry air mole fraction (totXCH4)

The totXCH4 is calculated dividing the CH$_4$ total column by the Dry Pressure Column (DPC) above Izaña. The DPC is calculated converting the ground pressure to column air concentration:

$$DPC = \frac{P_s}{m_{dry\ air} \cdot g(\varphi)} - \frac{m_{H_2O}}{m_{dry\ air}} \times H_2O_{col} \qquad (2)$$

being $P_s$ the surface pressure at Izaña ground level, $m_{dry\ air}$ the molecular mass of the dry air (~28.96 g mol$^{-1}$), $m_{H_2O}$ the molecular mass of the water vapor (~18 g mol$^{-1}$), $H_2O_{col}$ the water vapor total column amount (retrieved with a dedicated H$_2$O retrieval, Schneider, et al., 2010b), and $g(\varphi)$ the latitude dependent surface acceleration due to gravity. The ground pressure was acquired with a Setra System (precision of ±0.3 hPa).

#### 3.3.2 A posteriori corrected total column averaged mole fraction (troXCH4$_{post}$)

Similar to Washenfelder et al. (2003) we calculate the troXCH4$_{post}$ from the CH$_4$ total column after correcting the variation in both surface pressure and stratospheric contribution:

$$troXCH4_{post} = \frac{CH_{4_{col}} - b \cdot HF_{col}}{DPC} \qquad (3)$$

where $CH_{4_{col}}$ is the CH$_4$ total column from the scaling retrieval, $HF_{col}$ is the HF total column, and $b$ is the stratospheric slope equilibrium relationship between the CH$_4$ and HF columns. The coefficent $b$ is determined by vertically shifting the CH$_4$ and HF WACCM profiles (for details see Appendix A).

In Eq. (3) we apply a de-trended HF total column time series retrieved from the FTIR measurements at Izaña. The HF trend and annual cycle was calculated by fitting the following function to the HF daily mean time series:

$$f(t) = a_1 + a_2 t + \sum_{j=1}^{2} \left[ d_j \cos\left(k_j t\right) + e_j \sin\left(k_j t\right) \right] \tag{4}$$

where $t$ is the time in days; $a_1$ is a constant value, $a_2$ is the parameter of the linear trend and $d_j$ and $e_j$ are the parameters of the annual cycle ($k_j = 2\pi j / T$ with $T = 365.25$ days). Subtracting $a_2 t$ from the HF time series yields the de-trended HF time series. HF is believed to originate in the middle atmosphere solely from the photodissociation of man-made chlorofluorocarbons (CFCs) and hydrochlorofluorocarbons (HCFCs). The de-trending is performed in order to reduce the influence of the chemical variability of HF in the calculations. But it must be said that the whole HF chemical variability cannot be removed by de-trending. Finally, the variable Fluorine partitioning between HF and $COF_2$ introduces additional uncertainty into the HF post-correction approach.

### 3.3.3 Directly retrieved tropospheric column averaged volume mole fraction (troXCH4$_{retr}$)

The retrieval code PROFFIT is able to perform profile inversion and we can directly retrieve tropospheric $CH_4$ concentration profiles from the measured spectra. We use the retrieved concentration profiles to obtain a tropospheric column averaged $CH_4$ mole fraction directly from the measured spectra (troXCH4$_{retr}$). Therefore, we average the retrieved $CH_4$ volume mixing ratios between Izaña ground level and an altitude of 6.5 km. The values retrieved at these altitudes are well sensitive to free tropospheric $CH_4$ and are not affected by stratospheric $CH_4$ (see also next Sect. 3.4.2).

## 3.4 Characteristics of the FTIR CH$_4$ data

### 3.4.1 Error estimation

The error calculations presented here apply the error estimation capability incorporated in the PROFFIT retrieval algorithm. This computationally efficient implementation allows performing a reasonably complete estimate of the total error budget for each individual measurement. It is based on the analytic error estimation approach of Rodgers (2000). We assume the uncertainty sources as listed in Table 2. To avoid a too optimistic systematic error budget, both a statistical as well as a systematical contribution is allowed for each error source. We assume that 80 % of the uncertainties are random and 20 % systematic, respectively. Exceptions are the spectroscopic line parameter uncertainty (line strength and pressure broadening), which is assumed to be purely systematic, and the error due to spectral measurement noise, which is assumed to be purely statistical.

The estimated random and systematic errors for the scaling retrieval are listed in Table 3. While the uncertainty in the spectroscopic parameter determines the systematic error the baseline/continuum uncertainty is dominating the random error sources listed in Table 2.

In addition to these parameter errors we have to consider errors caused by the variability in the CH$_4$ profile shape. Generally the shape of the actual atmospheric CH$_4$ will differ from the shape of the scaled WACCM CH$_4$ profile. This gives rise to so-called smoothing error, which can be calculated as $(\mathbf{I} - \mathbf{A})\mathbf{S}_a(\mathbf{I} - \mathbf{A})^T$. Here $\mathbf{I}$ is a unity matrix, $\mathbf{A}$ is the averaging kernel, and $\mathbf{S}_a$ the assumed a priori covariance of atmospheric CH$_4$. Here we use a $\mathbf{S}_a$ matrix that is obtained from the WACCM simulations. We find that the smoothing error is by far the leading random error and thus determines the precision of totXCH4 produced by the scaling retrieval. When considering the smoothing error we estimate an overall precision of about 0.51 %.

Full Screen / Esc

The estimated random and systematic errors for the profile retrieval are shown in Fig. 3a–c respectively. Figure 3d shows the WACCM a priori CH$_4$ profile in order to have a reference. We observe that in the troposphere the random errors are dominated by instrumental specific uncertainty sources: the baseline offset uncertainty and the measurement noise. The total estimated random error due to parameter uncertainties is depicted as yellow line in Fig. 3a. It is about 17 ppb (0.9 % with respect to the WCCAM profile) in the lower troposphere and about 10 ppb (0.7 %) in the UT/LS region. In the stratosphere the smoothing error becomes the leading random error component.

Concerning systematic errors spectroscopic parameters are the dominating uncertainty sources. The estimated total systematic error is depicted as yellow line in Fig. 3c. It is about 65 ppb (3.6 %) and 100 ppb (7.1 %) for the lower troposphere and the UT/LS region respectively.

Table 4 collects the total systematic and random errors for our total $X$CH$_4$ product (totXCH4) and the a posteriori calculated tropospheric $X$CH$_4$ (troXCH4$_{post}$) as obtained from the scaling retrieval (SR). Furthermore, it shows the errors for the directly retrieved tropospheric $X$CH$_4$ (troXCH4$_{retr}$) and totXCH4 obtained from the profile retrieval (PR). For these calculations we assume the following uncertainties: 0.3 hPa for the surface pressure, 2.7 % for the HF column (Schneider et al., 2005), 1 % for the H$_2$O column (Schneider et al., 2010a), and 10 % for the $b$-value.

Theoretically, the scaling retrieval produces total column-averaged CH$_4$ (totXCH4) and a posteriori corrected tropospheric column-averaged CH$_4$ (troXCH4$_{post}$) with a precision of 0.51 % and 0.57 %, respectively (square root of the square sum of the smoothing error, measurement noise and the statistical error). By applying a profiling retrieval we can significantly reduce the smoothing error, which theoretically improves the precision of totXCH4 to 0.41 %. The directly retrieved tropospheric column-averaged CH$_4$ (troXCH4$_{retr}$) has an estimated precision of 0.91 %. Please note that the precision estimate for the a posteriori calculated tropospheric $X$CH$_4$ (troXCH4$_{post}$) is very likely too optimistic since we assume an uncertainty of the $b$-value applied in Eq. (3) of only 10 %, whereas the model-deduced HF-CH$_4$ correlation might be afflicted with a larger

uncertainty.

## 3.4.2 Characteristics of the retrieved CH$_4$ profiles

When retrieving vertical profiles it is important to document the vertical resolution that can be achieved with the remote sensing system. The vertical information contained in the FTIR profile is characterized by the averaging kernel matrix (**A**). This matrix depends on the retrieved parameters, the quality of the measurement (the signal to noise ratio), the spectral resolution, the solar zenith angle, etc. The averaging kernel matrix describes the smoothing of the real vertical distribution of the absorber by the FTIR measurements process. Figure 4 shows the rows of a typical averaging kernel matrix of our CH$_4$ retrieval. The row kernels indicate the altitude regions that mainly contribute to the retrieved state. The first atmospheric levels (from Izaña ground level up to 6.5 km) are highlighted by red colour showing that for the CH$_4$ mole fractions retrieved at these altitudes there is no significant contribution from the stratosphere. The respective mixing ratios are well representative for the free troposphere and we calculate our troXCH4$_{retr}$ as the average of the mole fractions at these altitudes. By the green colour we highlight the row kernel for an altitude of 21 km. We observe that the mole fractions values retrieved at 21 km well reflect the upper troposphere/lower stratosphere (UT/LS) region.

The trace of the averaging kernel matrix can be interpreted as the degree of freedom (DOF) of the measurement. The higher the value the more information is obtained from the measurement. A typical DOF value obtained for our CH$_4$ retrieval is 2.5.

## 4 Empirical validation

### 4.1 Intercomparison between the Bruker spectrometers IFS 120M and IFS 125HR

The Bruker spectrometers IFS 120M and IFS 125HR were operated side-by-side during March–April of 2005. On 17 days both instruments measured in coincidence and we can use these period for empirically documenting the errors caused by instrument specific random uncertainties. In case of the profile retrieval such instrument specific random uncertainties (baseline offset and measurement noise) dominate the total random error and we can use the side-by-side instrument intercomparison as an empirical validation of the overall precision. Table 5 shows a statistics of the intercomparison of the different $CH_4$ products obtained from the scaling and the profile retrieval. Concerning the profile retrieval (marked as PR) we find scatter values of 0.3 % for totXCH4 and 0.5 % for troXCH4$_{retr}$, thereby empirically documenting the good precision of this data. Concerning the scaling retrieval (marked as SR) the scatter values are even smaller, however it is important to note that in this case the smoothing error cancels out, since it is very similar for both instruments.

### 4.2 FTIR versus surface in-situ GAW data

As already mentioned in Sect. 2.1 the in-situ night-time data are well representative of free troposphere background conditions. Therefore, we compare the average of two consecutive in-situ night-time means with the mean of the FTIR data obtained during the enclosed day. We limit this study to the 2001–2010 period, since in 1999–2000 we find an inconsistency in the surface pressure data. Due to this inconsistency we are not able to calculate consistent DPC values for the 1999–2000 period (for more details see Appendix B).

The lower panel of Fig. 5 shows the daily means for totXCH$_4$ (dark green open triangles for the profiling retrieval, PR, and green solid squares for the scaling retrieval,

Title Page

Abstract | Introduction

Conclusions | References

Tables | Figures

◄ | ►

◄ | ►

Back | Close

Full Screen / Esc

Printer-friendly Version

Interactive Discussion

SR) and GAW CH$_4$ in-situ values (black points). The upper panel depicts the relative difference between FTIR and GAW data ((FTIR-GAW)/GAW, grey open triangles for PR and dark grey solid squares for SR). For the scaling retrieval we find a mean and standard deviation of the difference of $-4.69\,\% \pm 1.42\,\%$. The FTIR/GAW scaling factor is 0.9531. We find no significant correlation between the FTIR and GAW data (Correlation coefficient $R = 0.09$). In order to reduce the scatter caused by comparing different airmasses (we compare nighttime with daytime data) we perform an additional comparison of monthly mean data (graphic not shown). There the difference between the FTIR and GAW data is $-5.05\,\% \pm 1.28\,\%$ and the scaling factor 0.9495. Using monthly averages instead of daily mean data does not significantly reduce scatter and the bias between the two data sets. For the profiling retrieval we find a better agreement: mean and scatter of $-3.90\,\% \pm 1.06\,\%$ and $-4.17\,\% \pm 0.92\,\%$ for daily and monthly mean differences, respectively. The FTIR/GAW scaling factor is 0.9610 (daily mean). The results of this daily and monthly mean intercomparison between the GAW data and the FTIR products are collected in Tables 6 and 7.

The lower panel of Fig. 6 shows daily means GAW data (black circles) and the troXCH4$_{post}$ data (violet open squares). In the upper panel the relative FTIR-GAW difference is shown. We obtain a mean difference and scatter of $-2.69\,\% \pm 1.29\,\%$ (FTIR/GAW scaling factor of 0.9731). The correlation plot provides a rather low correlation coefficient of 0.18 (see Table 6). For the monthly mean comparison there is no significant change: correlation coefficient (0.16) and the relative FTIR-GAW scatter decreases to 1.16 % (see Table 7).

The NDACC spectra contain sufficient information to retrieve a CH$_4$ concentration profile with the characteristics that are described by the averaging kernels of Fig. 4. Theoretically we should be able to distinguish tropospheric from stratospheric CH$_4$. Figure 7 shows a time series of the CH$_4$ profiles retrieved from the FTIR measurements between 2001 and 2010. CH$_4$ concentrations are high in the troposphere and significantly decrease in the stratosphere where CH$_4$ is effectively destroyed by reaction with OH, Cl, and O($^1$D). In the CH$_4$ profile time series we can clearly observe the

upward shift of the UT/LS region during the summer months: in winter above 18 km the $CH_4$ concentrations are typically smaller than 1600 ppb, whereas in summer 1600 ppb are still achieved at an altitude of 20 km. Vice versa to $CH_4$, the HF concentrations are very small in the troposphere and start to increase significantly as function of altitude in
5  the stratosphere (HF is produced in the stratosphere by photolysis of CFCs). Similar to $CH_4$ in the UT/LS region the total column of HF is a good indicator for the stratospheric contribution. Indeed, we observe a strong anti-correlation between the HF amounts and the $CH_4$ mixing ratio at 21 km (altitude that is well representative for the UT/LS region, see Sect. 3.4.2). This strong anti-correlation ($R = -0.81$, see Fig. 8) confirms
10  the good quality of the $CH_4$ concentration retrieved for the UT/LS region.

The lower panel of Fig. 9 depicts the troXCH4$_{retr}$ time series (red stars) and in black circles the daily means GAW data. The upper panel depicts the respective relative FTIR-GAW difference. We get a mean and scatter of $-0.13\% \pm 0.97\%$ and a correlation coefficient of 0.60. For the monthly mean comparison the correlation further
15  improves (coefficient of 0.69) and the relative FTIR-GAW scatter decreases to 0.69 % (see Tables 6 and 7). The good correlation between the GAW data and the tropospheric FTIR $CH_4$ concentrations, on the one hand, and the strong anti-correlation between the HF columns and the UT/LS FTIR $CH_4$ concentrations document the good quality of the retrieved $CH_4$ profiles. The NDACC FTIR systems allow measuring tropospheric $CH_4$
20  independently from stratospheric $CH_4$. Furthermore, the FTIR/GAW scaling factor for troXCH4$_{retr}$ is very close to unity (it is 0.9987, see Table 6) indicating that the applied $CH_4$ HITRAN 2008 line strength parameters are in good absolute agreement to the GAW $CH_4$ experiments. The troXCH4$_{retr}$ and the GAW datasets are consistent and could be used in a synergetic manner in flux inversion models.
25  Figure 10 shows the troXCH4$_{retr}$/<SF> versus $CH_{4_{GAW}}$ (being <SF> the mean scaling factor between troXCH4$_{retr}$ and $CH_{4_{GAW}}$). We observe that the slope of the linear regression line is smaller than unity: the fitted linear function goes from 20 ppb above the diagonal to 20 ppb below the diagonal. This is in agreement with the column sensitivity of the FTIR retrieval being smaller than 1.0 in the lower part of the troposphere ($\sim$0.8;

graphic not shown), i.e. the FTIR system does not capture the whole $CH_4$ variation. However, Fig. 10 might also suggest that the troXCH4$_{retr}$ and the GAW datasets are not fully equivalent because the former applies for the tropospheric column, whereas the latter applies only for the lower part of the free troposphere. The $CH_4$ variability might be larger in the lower part of the free troposphere than in the upper part of the free troposphere.

## 4.3 Interannual trend

We analyzed the $CH_4$ interannual trend for the FTIR and surface in-situ values. For estimating the interannual trend we calculate yearly mean data. However, since sampling is not uniform and there might be years with more measurements than usual during a certain season we have to subtract the annual cycle (de-seasonalise the time series). We estimate the annual cycle by fitting the following function to the time series:

$$f(t) = a_1 + a_2 t + \sum_{i=1}^{4} [b_i \cos(w_i t) + c_i \sin(w_i t)] + \sum_{j=1}^{2} [d_j \cos(k_j t) + e_j \sin(k_j t)] \quad (5)$$

where $t$ is the time in days; $a_1$, $a_2$, $b_i$ and $c_i$ are the parameters of the interannual trend and $d_j$ and $e_j$ are the parameters of the annual cycle, all of them to be determined; $w_i = 2\pi i/N$ being $N$ equals the number of days in the considered period and $k_j = 2\pi j/T$ with $T = 365.25$ days. The de-seasonalised time series can then be used to calculate the yearly mean time series. The yearly mean time series of $CH_{4_{GAW}}$ and of the different FTIR products are shown in Fig. 11: in Fig. 11a for totXCH4 from the scaling retrieval (SR) and the profiling retrieval (PR) and in Fig. 11b for the troXCH4 products. Beside troXCH4$_{post}$ and troXCH4$_{retr}$ we show here troXCH4$_{retr\_gbm}$, which is the same as troXCH4$_{retr}$ but applying the spectral microwindows, retrieval settings and line lists recommended by Sussmann et al. (2011). For all datasets we observe that before 2005 the $CH_4$ concentrations remained stable and after 2005 there has been a continuous $CH_4$ increase. Although a detailed discussion of this trend is beyond the

**Long-term validation of total and tropospheric $CH_4$ mole fractions**

E. Sepúlveda et al.

scope of this paper we would like to mention that our results are in excellent agreement with those of Dlugokencky et al. (2009) and Rigby et al. (2008).

In order to assess how the yearly mean time series of the different FTIR products agree with the corresponding GAW time series we calculate the random mean square between the yearly mean GAW data and the yearly mean FTIR data. The results are collected in Table 8. The different FTIR products agree similarly well with the GAW data. The troXCH4$_{retr\_gbm}$ results agree slightly poorer.

In Table 9 we collect the change in mean CH$_4$ VMR between the 2001–2003 and the 2008–2010 period. The GAW concentrations (CH$_{4_{GAW}}$) changed by about 20 ppb. This change is slightly overestimated by all the FTIR data products. However, this overestimation is not significant. It is within the 1 $\sigma$ uncertainty range. We find that the directly retrieved tropospheric column averaged CH$_4$ shows the best agreement with the GAW dataset.

## 4.4 De-trended CH$_4$ annual cycle

We compare the annual CH$_4$ cycles of the GAW data and of the different FTIR CH$_4$ products. Therefore, we de-trend the CH$_4$ time series. This de-trending is performed by removing the interannual trends as depicted in Fig. 11. Figure 12 shows the de-trended monthly means calculated for the 2001–2010 period: black circles for the GAW data, green solid squares and dark green open triangles for totXCH4 obtained from the scaling and profiling retrieval, respectively (see Fig. 12a), violet open squares for troXCH4$_{post}$, red stars for troXCH4$_{retr}$, and dark yellow open stars for troXCH4$_{retr\_gbm}$. All the annual cycles have been centered to zero.

We observe that totXCH4 does not reproduce the tropospheric surface in-situ CH$_4$ variability. It is obvious that totXCH4 is not a good proxy for the tropospheric seasonal CH$_4$ variability. Instead the totXCH4 annual variability is dominated by the annual variability of the tropopause height, which is lowest by the end of winter and continuously increases during summer. The totXCH4 cycle obtained from the scaling retrieval differs significantly from the totXCH4 cycle obtained from the profile retrieval. This implies

that the smoothing error – which is very important for a scaling retrieval with fixed first guess profile shape – depends on the season.

Similar to the totXCH4 cycle the troXCH4$_{post}$ cycle does not capture the minimum during summer and the maximum in the early winter. Instead it follows more or less the annual cycle of the tropopause altitude. We observe that the a posteriori correction method cannot adequately account for the stratospheric contribution.

On the contrary the troXCH4$_{retr}$ cycle is in very consistent to the GAW in-situ cycle. The amplitudes and phases of both cycles are very similar thereby confirming that the directly retrieved tropospheric column-averaged $X$CH$_4$ values are a very good proxy for the free tropospheric CH$_4$ concentrations. This is in particularly true when applying our retrieval settings. The retrieval setup suggested by Sussmann et al. (2011) fails to improve the reconstruction of the annual cycle.

## 5 Outlook and conclusions

In the framework of the NDACC ground-based FTIR experiments have recorded high resolution mid-infrared solar absorption spectra for more than a decade at about 15 globally distributed sites. We examine two different CH$_4$ retrieval principles: first, a simple scaling of a fixed climatologic profile and second a CH$_4$ profile retrieval.

A scaling retrieval is indicated if there is no significant variation in the profile shape or if the variations in the profile shape are not reflected in the measured solar absorption spectra (e.g. due to limited spectral resolution or measurement noise). However, our study shows that the high quality NDACC spectra contain significant information about the typical vertical variability of CH$_4$ converting the smoothing error in the leading error component of the scaling retrieval. We estimate a theoretical precision of the total $X$CH$_4$ of 0.51 %. The smoothing error of total $X$CH$_4$ can be significantly reduced if performing a profile retrieval leading to an improved precision of 0.41 %. This good precision is empirically confirmed by a side-by-side intercomparison study applying two FTIR instruments in 2005. We document that only the profile retrieval produces

total $X$CH$_4$ with high precision and should be used for producing data for scientific applications. We find, for instance, the annual $X$CH$_4$ cycle obtained by the scaling retrieval significantly differs from the cycle obtained by the profile retrieval.

While precise total $X$CH$_4$ FTIR data are an important reference for the validation of space-base $X$CH$_4$ experiments (e.g. SCIAMACHY, GOSAT, OCO-2), the total $X$CH$_4$ amounts are significantly affected by the variability of the stratospheric CH$_4$ contribution. We document that the annual cycle of total $X$CH$_4$ rather follows the annual cycle of the tropopause altitude and not the annual cycle of tropospheric CH$_4$ mole fraction. Our study shows that total $X$CH$_4$ is no valid proxy for tropospheric CH$_4$.

We investigate two methods for obtaining a tropospheric CH$_4$ proxy from the FTIR measurements. First, the often applied a posteriori correction method, which applies a CH$_4$ scaling retrieval and a posteriori corrects the stratospheric CH$_4$ constribution using HF total column amounts as stratospheric CH$_4$ proxy. This data set is called troXCH4$_{post}$ througout the paper. Second, we directly retrieve tropospheric column-averaged $X$CH$_4$ amounts from the spectra applying the profile retrieval. This data set is called troXCH4$_{retr}$ throughout paper.

Concerning troXCH4$_{post}$ we estimate a precision of 0.57 %. However, this estimation cannot be empirically confirmed by our comparison to the GAW CH$_4$ in-situ data (the scatter between CH$_{4_{GAW}}$ and troXCH4$_{post}$ is as large as 1.29 %). The reason might be an underestimation of the smoothing error, a too optimistic assumption of the uncertainty of the $b$-value, or a seasonal variability of the Fluorine partitioning. The scientific usefulness of troXCH4$_{post}$ data is rather doubtful. For instance, it does not captures the full amplitude of the tropospheric CH$_4$ annual cycle.

For troXCH4$_{retr}$ we estimate a theoretical precision of 0.91 %. This value is consistent with the results of the side-by-side FTIR intercomparison study of 2005 and it is well confirmed by the comparison to the GAW CH$_4$ in-situ data (we obtain a scatter between CH$_{4_{GAW}}$ and troXCH4$_{retr}$ of 0.97 %). Furthermore, we found that the FTIR/GAW scaling factor is very close to unity, suggesting that the NDACC FTIR network can provide tropospheric column-averaged CH$_4$ that is very consistent to the CH$_4$ data

Title Page

Abstract | Introduction

Conclusions | References

Tables | Figures

|◄ | ►|

◄ | ►

Back | Close

Full Screen / Esc

Printer-friendly Version

Interactive Discussion

of the GAW in-situ network. The annual cycle of troXCH4$_\text{retr}$ and CH4$_\text{GAW}$ are very similar (phase and amplitude). For investigating the CH$_4$ interchange between atmosphere, biosphere, and ocean, we strongly recommend using the directly retrieved tropospheric $X$CH$_4$ instead of the tropospheric $X$CH$_4$ produced by the a posteriori correction method.

Due to its long-term characteristics the NDACC tropospheric $X$CH$_4$ data set can make valuable contributions when investigating sources and sinks of CH$_4$. In the future we will examine CH$_4$ profile retrievals in the near infrared spectral region, which is recorded by the TCCON experiments. We will examine the practicability and benefits of a profile retrieval for obtaining highly precise total column-averaged $X$CH$_4$ amounts from TCCON spectra. Furthermore, we will use the Izaña GAW CH$_4$ in-situ data set for documenting the precision of possible TCCON tropospheric column-averaged CH$_4$ data and its level of consistency to the GAW CH$_4$ in-situ data.

## Appendix A

### Using HF column amounts as proxy for the tropopause altitude

The black solid lines in Fig. A1 show the climatology of modeled mixing ratio profiles (left panel for CH$_4$ and right panel for HF). We now want to estimate how a vertical shift of the profiles affects the total column amounts of the two trace gases. Therefore, we shift the two profiles between −5 km and +5 km and calculate the respective total column amounts.

Figure A2 shows the total column amounts of HF for the different shifts versus the respective amounts of CH$_4$. As expected we see a clear anti-correlation: for a positive shift (upward shift) CH$_4$ column amounts increase and HF column amounts decrease. For a negative shift (downward shift) it is vice versa. Due to this strong anti-correlation we can use the HF column amounts as a proxy for the changes in the CH$_4$ column

amounts caused by changes of the tropopause altitude. We find a slope of the fitted regression line of −554 (linear least squares fit). This slope value is applied as *b*-value in Eq. (3).

## Appendix B

### Surface pressure measurements at Izaña observatory

The 1999–2010 surface pressure measurements time series presents a jump at the beginning of 2001. The reason is that before and after 2001 two different types of pressure sensor have been applied: until 2001 a Thyas sensor ($\sim \pm 1$ hPa) and since 2001 a Setra sensor ($\pm 0.3$ hPa). Furthermore, the sensors were located at different positions and altitudes.

Figure B1 shows the time series of the daily mean pressure values acquired from both sensors at Izaña station. This jump will propagate into the totXCH4 and troXCH4$_{post}$ with about 7 ppb and 8 ppb, respectively. Therefore, we decided to present CH$_4$ time series only from 2001 onward.

# References

Bousquet, P., Ringeval, B., Pison, I., Dlugokencky, E. J., Brunke, E.-G., Carouge, C., Chevallier, F., Fortems-Cheiney, A., Frankenberg, C., Hauglustaine, D. A., Krummel, P. B., Langenfelds, R. L., Ramonet, M., Schmidt, M., Steele, L. P., Szopa, S., Yver, C., Viovy, N., and Ciais, P.: Source attribution of the changes in atmospheric methane for 2006–2008, Atmos. Chem. Phys., 11, 3689–3700, doi:10.5194/acp-11-3689-2011, 2011.

Dlugokencky, E. J., Bruhwiler, L., White, J. W. C., Emmons, L. K., Novelli, P. C., Montzka, S. A., Masarie, K. A., Lang, P. M., Crotwell, A. M., Miller, J. B., and Gatti, L. V.: Observational constraints on recent increases in the atmospheric $CH_4$ burden, Geophys. Res. Lett., 36, L18803, doi:10.1029/2009GL039780, 2009.

Frankenberg, C., Meirink, J. F., van Weele, M., Platt, U., and Wagner, T.: Assessing methane emissions from global spaceborne observations, Science, 308, 1010–8438, 2005.

Frankenberg, C., Aben, I., Bergamaschi, P., Dlugokencky, E. J., van Hees, R., Houweling, S., van der Meer, P., Snel, R., and Tol, P.: Global column-averaged methane mixing ratios from 2003 to 2009 as derived from SCIAMACHY: Trends and variability, J. Geophys. Res., 116, D04302, doi:10.1029/2010JD014849, 2011.

Gardiner, T., Forbes, A., de Mazière, M., Vigouroux, C., Mahieu, E., Demoulin, P., Velazco, V., Notholt, J., Blumenstock, T., Hase, F., Kramer, I., Sussmann, R., Stremme, W., Mellqvist, J., Strandberg, A., Ellingsen, K., and Gauss, M.: Trend analysis of greenhouse gases over Europe measured by a network of ground-based remote FTIR instruments, Atmos. Chem. Phys., 8, 6719–6727, doi:10.5194/acp-8-6719-2008, 2008.

Gomez-Pelaez, A. J., Ramos, R., Cuevas, E., and Gomez-Trueba, V.: 25 years of continuous $CO_2$ and $CH_4$ measurements at Izaña Global GAW mountain station: annual cycles and interannual trends; Proceedings of the Symposium on Atmospheric Chemistry and Physics at Mountain Sites, ACP Symposium 2010, 8–10 June 2010, http://www.izana.org/publications/Abstract_25-year_CO2_and_CH4_Izana.pdf, last access: 2 February 2012, Interlaken, Switzerland, 157–159, 2010.

Gomez-Pelaez, A. J. and Ramos, R.: Improvements in the Carbon Dioxide and Methane Continuous Measurement Programs at Izaña Global GAW Station (Spain) during 2007–2009, Report of the 15th WMO/IAEA Meeting of Experts on Carbon Dioxide, Other Greenhouse Gases, and Related Tracer Measurement Techniques, 7–10 September 2009, GAW Report number 194, WMO TD 1553, http://www.wmo.int/pages/prog/arep/gaw/gaw-reports.html,

last access: 2 February 2012, Jena, Germany, 330 pp., 2011.

Gomez-Pelaez, A. J., Ramos, R., Gomez-Trueba, V., Campo-Hernandez, R., Dlugokencky, E., and Conway, T.: New improvements in the Izaña (Tenerife, Spain) global GAW station in-situ greenhouse gases measurement program; to be published in the proceedings of the 16th WMO/IAEA Meeting on Carbon Dioxide, Other Greenhouse Gases, and Related Measurement Techniques 25–28 October 2011, GAW Report to be publish, Wellington, New Zealand, 2012.

Hase, F.: Inversion von Spurengas-profilen aus hochaufgelösten bodengebundenen FTIR-Messungen in Absorption, FZKA 6512, Forschungszentrum Kalrsruhe, 2000.

Hase, F.: Interactive comment on "Strategy for high-accuracy-and-precision retrieval of atmospheric methane from the mid-infrared FTIR network" by R. Sussmann et al., Atmos. Meas. Tech. Discuss., 4, C1048–C1048, 2011.

Hase, F., Blumenstock, T., and Paton-Walsh, C.: Analysis of the instrumental line shape of high-resolution Fourier transform IR spectrometers with gas cell measurements and new retrieval software, Appl. Optics, 38, 3417–3422, 1999.

Hase, F., Hannigan, J. W., Coffey, M. T., Goldman, A., Höpfner, M., Jones, N. B., Rinsland, C. P., and Wood, S. W.: Intercomparison of retrieval codes used for the analysis of high-resolution, ground-based FTIR measurements, J. Quant. Spectrosc. Ra., 87, 25–52, 2004.

IPCC: Climate Change 2007 – The Physical Science Basis: Contribution of Working Group I to the Fourth Assessment Report of the Intergovernmental Panel on Climate, Cambridge University Press, Cambridge, UK and New York, NY, USA, 2007.

Keppler, F., Hamilton, T. G., Braß, M., and Rockmann, T.: Methane emissions from terrestrial plants under aerobic conditions, Nature, 439, 187–191, doi:10.1038/nature04420, 2006.

Olsen, S. C. and Randerson, J. T.: Differences between surface and column atmospheric $CO_2$ and implications for carbon cycle research, J. Geophys. Res., 109, D02301, doi:10.1029/2003JD003968, 2004.

Rigby, M., Prinn, R. G., Fraser, P. J., Simmonds, P. G., Langenfelds, R. L., Huang, J., Cunnold, D. M., Steele, L. P., Krummel, P. B., Weiss, R. F., O'Doherty, S., Salameh, P. K., Wang, H. J., Harth, C. M., M¨uhle, J., and Porter, L. W.: Renewed growth of atmospheric methane, Geophys. Res. Lett., 35, L22805, doi:10.1029/2008GL036037, 2008.

Rodgers, C. D.: Inverse Methods for Atmospheric Sounding: Theory and Praxis, ISBN 981-02-2740-X, World Scientific Publishing Co., Singapore, 2000.

Rothman, L. S., Gordon, I. E., Barbe, A., Chris Benner, D., Bernath, P. F., Birk, M., Boudon,

Title Page

Abstract | Introduction

Conclusions | References

Tables | Figures

◄ | ►

◄ | ►

Back | Close

Full Screen / Esc

Printer-friendly Version

Interactive Discussion

V., Brown, L. R., Campargue, A., Champion, J.-P., Chance, K., Coudert, L. H., Dana, V., Devi, V. M., Fally, S., Flaud, J.-M., Gamache, R. R., Goldman, A., Jacquemart, D., Kleiner, I., Lacome, N., Lafferty, W. J., Mandin, J.-Y., Massie, S. T., Mikhailenko, S. N., Miller, C. E., Moazzen-Ahmadi, N., Naumenko, O. V., Nikitin, A. V., Orphal, J., Perevalov, V. I., Perrin, A., Predoi-Cross, A., Rinsland, C. P., Rotger, M., Simecková, M., Smith, M. A. H., Sung, K., Tashkun, S. A., Tennyson, J., Toth, R. A., Vandaele, A. C., and Vander-Auwera, J.: The HITRAN 2008 molecular spectroscopic database, J. Quant. Spectrosc. Ra., 110, 533–572, doi:10.1016/j.jqsrt.2009.02.013, 2009.

Schneider, M., Blumenstock, T., Chipperfield, M. P., Hase, F., Kouker, W., Reddmann, T., Ruhnke, R., Cuevas, E., and Fischer, H.: Subtropical trace gas profiles determined by ground-based FTIR spectroscopy at Izaña (28° N, 16° W): Five-year record, error analysis, and comparison with 3-D CTMs, Atmos. Chem. Phys., 5, 153–167, doi:10.5194/acp-5-153-2005, 2005.

Schneider, M., Hase, F., and Blumenstock, T.: Water vapour profiles by ground-based FTIR spectroscopy: study for an optimised retrieval and its validation, Atmos. Chem. Phys., 6, 811–830, doi:10.5194/acp-6-811-2006, 2006.

Schneider, M., Toon, G. C., Blavier, J.-F., Hase, F., and Leblanc, T.: $H_2O$ and $\delta D$ profiles remotely-sensed from ground in different spectral infrared regions, Atmos. Meas. Tech., 3, 1599–1613, doi:10.5194/amt-3-1599-2010, 2010a.

Schneider, M., Romero, P. M., Hase, F., Blumenstock, T., Cuevas, E., and Ramos, R.: Continuous quality assessment of atmospheric water vapour measurement techniques: FTIR, Cimel, MFRSR, GPS, and Vaisala RS92, Atmos. Meas. Tech., 3, 323–338, doi:10.5194/amt-3-323-2010, 2010b.

Sussmann, R., Forster, F., Rettinger, M., and Jones, N.: Strategy for high-accuracy-and-precision retrieval of atmospheric methane from the mid-infrared FTIR network, Atmos. Meas. Tech., 4, 1943–1964, doi:10.5194/amt-4-1943-2011, 2011.

Washenfelder, R. A., Wennberg, P. O., and Toon, G. C.: Tropospheric methane retrieved from ground-based near-IR solar absorption spectra, Geophys. Res. Lett., 30, L017969, doi:10.1029/2003GL017969, 2003.

Zellweger, C., Klausen, J., and Buchmann, B.: System and performance audit for surface ozone, carbon monoxide, methane and nitrous oxide at the global GAW station Izana, Spain, March 2009, http://gaw.empa.ch/audits/IZO_2009.pdf), last access: 2 February 2012, WCC-Empa Report 09/1, 2009.

Title Page

Abstract | Introduction

Conclusions | References

Tables | Figures

|◄ | ►|

◄ | ►

Back | Close

Full Screen / Esc

Printer-friendly Version

Interactive Discussion

**Table 1.** Spectral MicroWindows (MW) chosen for the CH$_4$ retrieval shown in this study.

| Spectral MicroWindows (cm$^{-1}$) | |
|---|---|
| MW1 | 2613.7000–2615.4000 |
| MW2 | 2650.6000–2651.3000 |
| MW3 | 2835.5000–2835.8000 |
| MW4 | 2903.6000–2904.0250 |

**Table 2.** Assumed random and systematic uncertainties. It is assumed that 80 % of the values listed in the table below correspond to random uncertainties and 20 % to systematic uncertainties (except for spectroscopy that is assumed to be 100 % systematic).

| Source | Uncertainty |
| --- | --- |
| Baseline/continuum (offset and channeling) | 0.1 % |
| Instrumental lines shape (modulation efficiency and phase error) | 1 % and 0.01 rad |
| Line of sight | 0.001 rad |
| Solar lines (intensity and spectral scale) | 1 % and 1.0E-6 |
| Temperature | 1.0 K (trop)/2.0 K (strat) |
| Spectroscopy (intensity strength and pressure broadening – $\gamma$air) | 2 % and 5 % |

Table 3. Errors for each parameter for the scaling retrieval for CH$_4$ total column.

| | Statistic error (%) | Systematic error (%) |
|---|---|---|
| Baseline/continuum | 0.23 | 6E-3 |
| Instrumental lines shape | 0.03 | 7E-3 |
| Line of sight | 0.06 | 7E-3 |
| Solar lines | 0.02 | 4E-3 |
| Temperature | 0.11 | 0.03 |
| Measurement noise | 0.08 | |
| Smoothing error | 0.43 | |
| Spectroscopy | | 3.59 |
| Total error | 0.51 | 3.59 |

**Table 4.** Total errors estimated for typical measurement conditions (16 June 2010).

| | | Typical value | Smoothing error | | Statistic error | | Systematic error | |
|---|---|---|---|---|---|---|---|---|
| | | ppb | % | ppb | % | ppb | % | ppb |
| SR | totXCH4 | 1743 | 0.43 | 7.50 | 0.27 | 4.71 | 3.50 | 61.01 |
| SR$^*$ | troXCH4$_{post}$ | 1790 | 0.43 | 7.70 | 0.37 | 6.62 | 3.41 | 61.11 |
| PR | totXCH4 | 1743 | 0.06 | 1.05 | 0.41 | 7.15 | 2.23 | 38.87 |
| PR | troXCH4$_{retr}$ | 1812 | 0.20 | 3.62 | 0.89 | 15.95 | 3.26 | 59.07 |

SR: Scale retrieval; PR: profile retrieval; SR$^*$: applying HF correction using the CH$_4$ total column from SR.

**Table 5.** Statistics of the daily mean comparisons between the side-by-side measuring instruments 120M and 125HR.

| | | $N$ | $R$ | MRD (%) | STD (%) | SF ± SEM |
|---|---|---|---|---|---|---|
| SR | totXCH4 | 17 | 0.91 | −0.17 | 0.28 | 0.9983 ± 0.0014 |
| SR$^*$ | troXCH4$_{post}$ | 17 | 0.73 | −0.14 | 0.27 | 0.9986 ± 0.0014 |
| PR | totXCH4 | 17 | 0.73 | −0.10 | 0.30 | 0.9990 ± 0.0015 |
| PR | troXCH4$_{retr}$ | 17 | 0.83 | 0.06 | 0.51 | 1.0006 ± 0.0025 |

$N$: number of data points; $R$: correlation coefficient; MRD: mean relative difference (120M–125HR)/125HR; STD: standard Deviation; SF: scaling factor (120M/125HR); SEM: standard error of the mean of the scaling factor = $2 \times$ STD/sqrt($N$); SR: Scale Retrieval; PR: Profile Retrieval; SR$^*$: applying HF correction using the CH$_4$ total column from SR.

**Table 6.** Statistics of the daily mean comparisons between the FTIR products (totXCH4, troXCH4$_{post}$, and troXCH4$_{retr}$) and the GAW data for the period 2001–2010.

|  | FTIR product | $N$ | $R$ | MRD (%) | STD (%) | SF ± SEM |
|---|---|---|---|---|---|---|
| SR | totXCH4 | 709 | 0.09 | −4.69 | 1.42 | 0.9531 ± 0.0011 |
| SR$^*$ | troXCH4$_{post}$ | 709 | 0.18 | −2.69 | 1.29 | 0.9731 ± 0.0010 |
| PR | totXCH4 | 709 | 0.39 | −3.90 | 1.06 | 0.9610 ± 0.0008 |
| PR | troXCH4$_{retr}$ | 709 | 0.60 | −0.13 | 0.97 | 0.9987 ± 0.0007 |

$N$: number of data points; $R$: correlation coefficient; MRD: mean relative difference (120M−125HR)/125HR; STD: standard Deviation; SF: scaling factor (120M/125HR); SEM: standard error of the mean of the scaling factor = 2 × STD/sqrt($N$); SR: Scale Retrieval; PR: Profile Retrieval; SR$^*$: applying HF correction using the CH$_4$ total column from SR.

**Table 7.** Same as Table 6 but for monthly means.

|     | FTIR product | N | R | MRD (%) | STD (%) | SF ± SEM |
|-----|--------------|-----|------|---------|---------|----------------------|
| SR  | totXCH4      | 98 | 0.09 | −5.05 | 1.28 | 0.9495 ± 0.0026 |
| SR* | troXCH4$_{post}$ | 98 | 0.16 | −3.03 | 1.16 | 0.9697 ± 0.0024 |
| PR  | totXCH4      | 98 | 0.40 | −4.17 | 0.92 | 0.9583 ± 0.0019 |
| PR  | troXCH4$_{retr}$ | 98 | 0.69 | −0.32 | 0.69 | 0.9968 ± 0.0014 |

**Table 8.** Root Mean Square (RMS) between the annual means (2001–2010 period) of GAW and the FTIR data (see Fig. 10).

| | CH$_{4_{GAW}}$ − $a$ | | | | |
|---|---|---|---|---|---|
| $a$ | totXCH4 (SR) | totXCH4 (PR) | troXCH4$_{post}$ (SR$^*$) | troXCH4$_{retr}$ (PR) | troXCH4$_{retr\_gbm}$ (PR) |
| RMS [ppb] | 5.15 | 4.52 | 4.72 | 4.81 | 7.51 |

SR: Scale retrieval; PR: profile retrieval; SR$^*$: applying HF correction using the CH$_4$ total column from SR.

**Table 9.** Difference between the mean CH$_4$ VMR in 2001–2003 and in 2008–2010 with its associated 1$\sigma$ uncertainty.

| dataset | CH$_{4_{GAW}}$ | totXCH4 (SR) | totXCH4 (PR) | troXCH4$_{post}$ (SR*) | troXCH4$_{retr}$ (PR) | troXCH4$_{retr\_gbm}$ (PR) |
|---------|----------------|--------------|--------------|------------------------|------------------------|----------------------------|
| Difference [ppb] | 19.65 ±5.00 | 26.46 ±9.19 | 25.61 ±4.74 | 26.98 ±8.05 | 22.79 ±5.12 | 26.79 ±4.91 |

SR: Scale retrieval; PR: profile retrieval; SR*: applying HF correction using the CH$_4$ total column from SR.
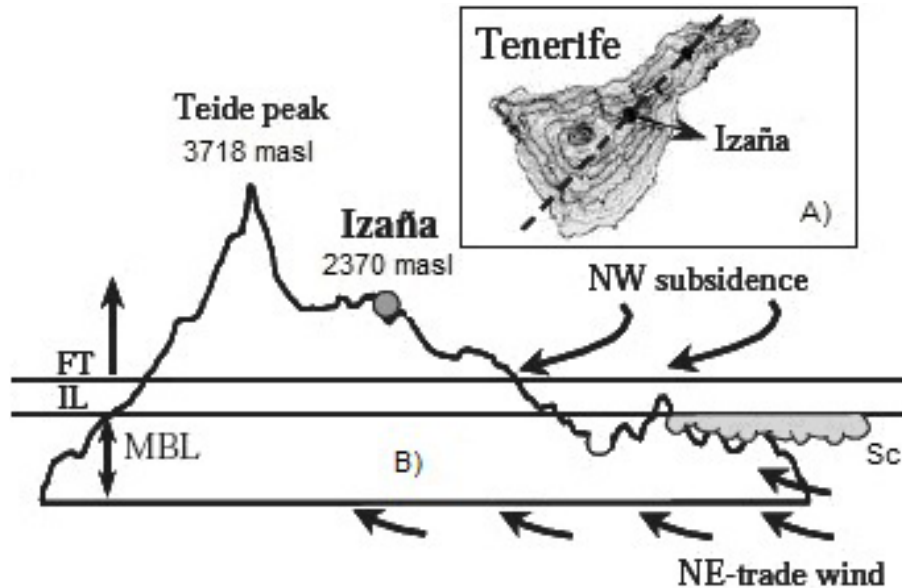
**Fig. 1. (A)** Location of Izaña in Tenerife Island, **(B)** transect of Tenerife Island – along the dotted line in **(A)** – showing the vertical stratification: MBL: marine boundary layer, IL: inversion layer, FT: free troposphere, Sc: stratocumulus.
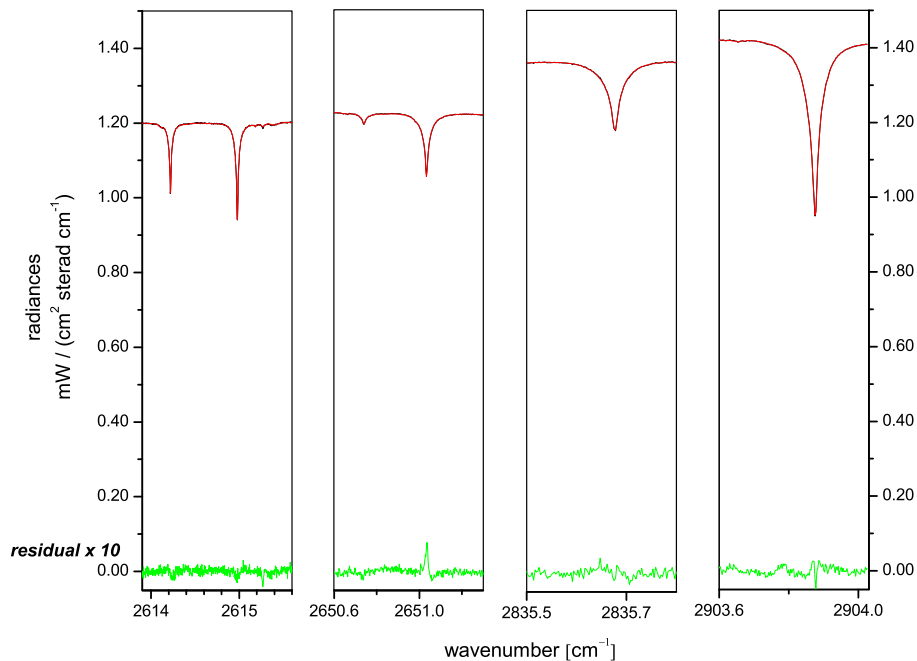
**Fig. 2.** The four applied spectral microwindows: measured spectrum (black), simulated spectrum (red), and residuals multiplied by a factor of 10 (green).
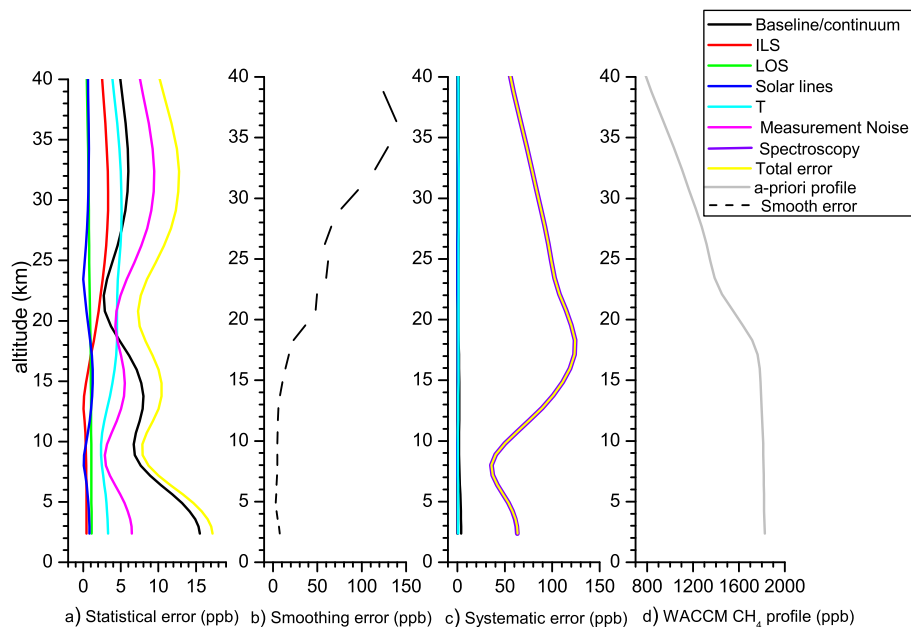
**Fig. 3.** Estimated errors for the profiling retrieval (PR): **(a)** statistical (random) errors of parameters listed in Table 2, **(b)** smoothing error, **(c)** systematic errors, and **(d)** climatologic CH$_4$ profile simulated by the WACCM model that is used as the a-priori profile. The different colours are for the different uncertainty sources as explained in the legend. The yellow line represents the total errors and the grey line is the WACCM profile.
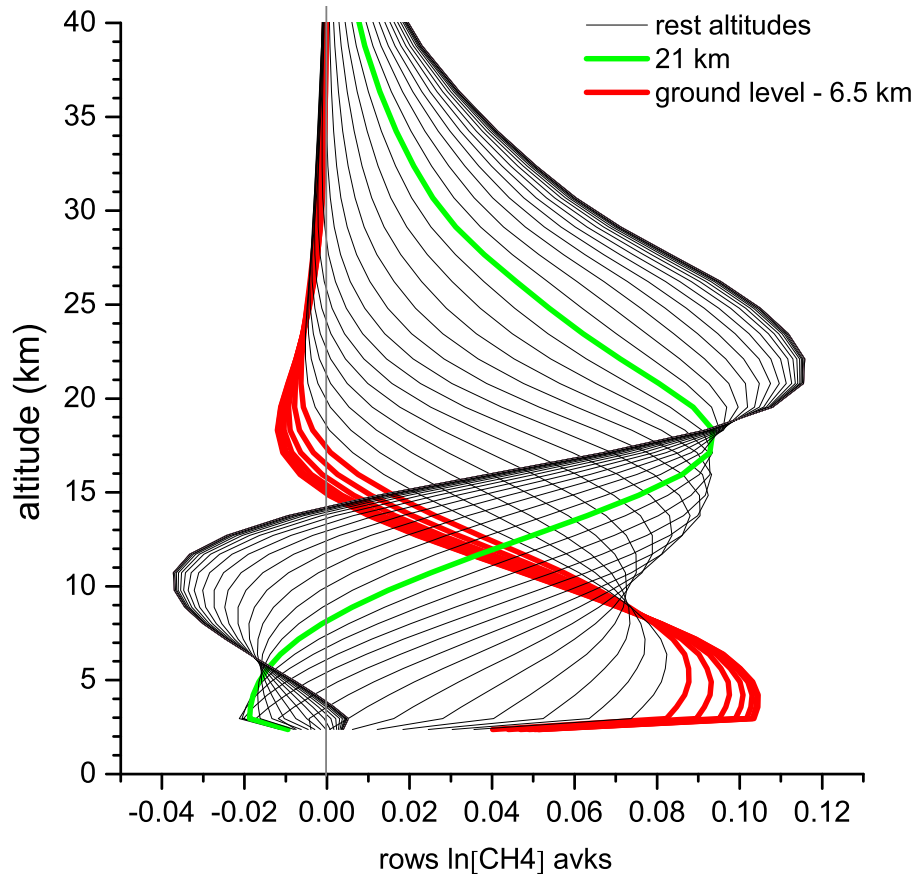
**Fig. 4.** Typical row averaging kernels for profiling retrieval (PR): red lines show the kernels between Izaña ground level and 6.5 km while the green line shows the kernel corresponding to an altitude of 21 km.
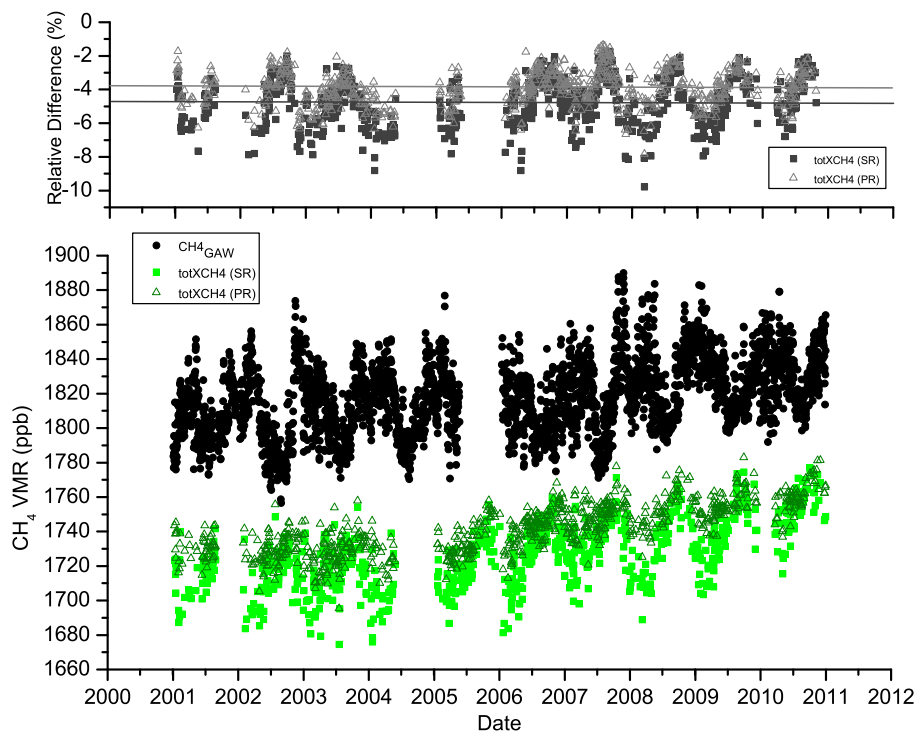
**Fig. 5.** CH$_{4_{GAW}}$ in-situ (black circles) and totXCH4 FTIR data obtained from scaling (squares) and profiling (triangles) retrieval, respectively. Bottom panel: 2001–2010 time series for all available data; top panel: time series of the difference expressed as (FTIR-GAW)/GAW for the scaling (squares) and profiling (triangles) retrieval, respectively. The solid lines represent the mean relative difference for the scaling and profiling retrieval, respectively.
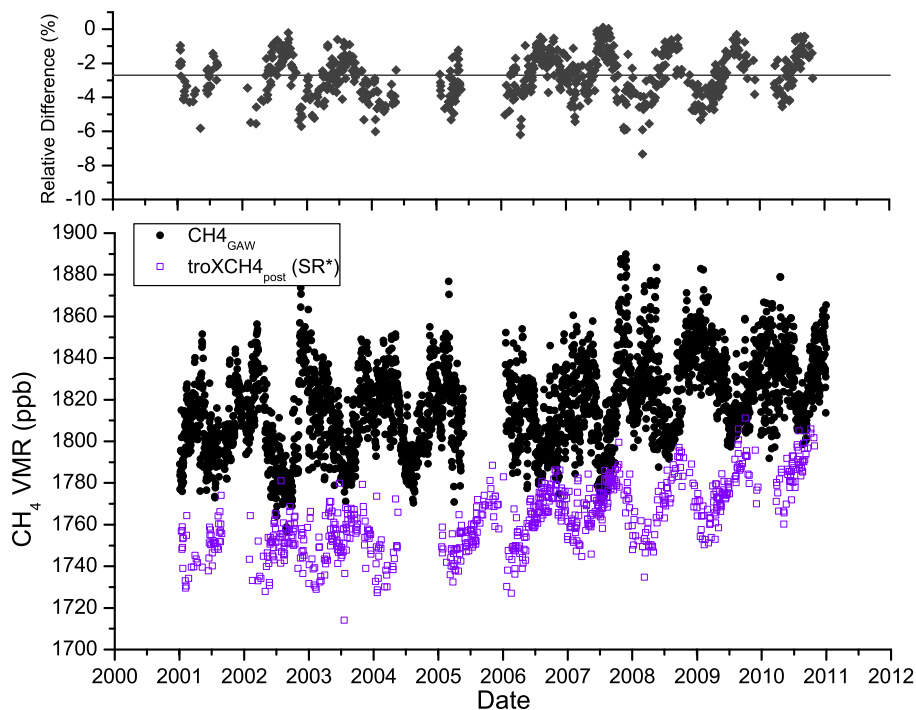
**Fig. 6.** Same as Fig. 5, but for the a posteriori corrected tropospheric $X$CH$_4$ calculated from the total CH$_4$ column obtained from the scaling retrieval and applying the HF correction (troXCH4$_{post}$, violet empty squares).
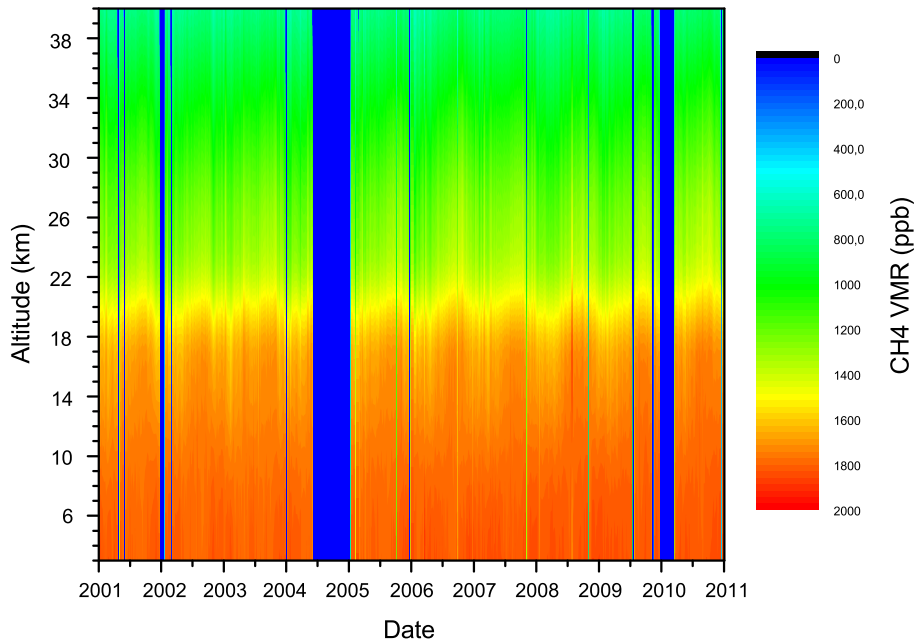
**Fig. 7.** Retrieved CH$_4$ profile time series for the period 2001–2010.
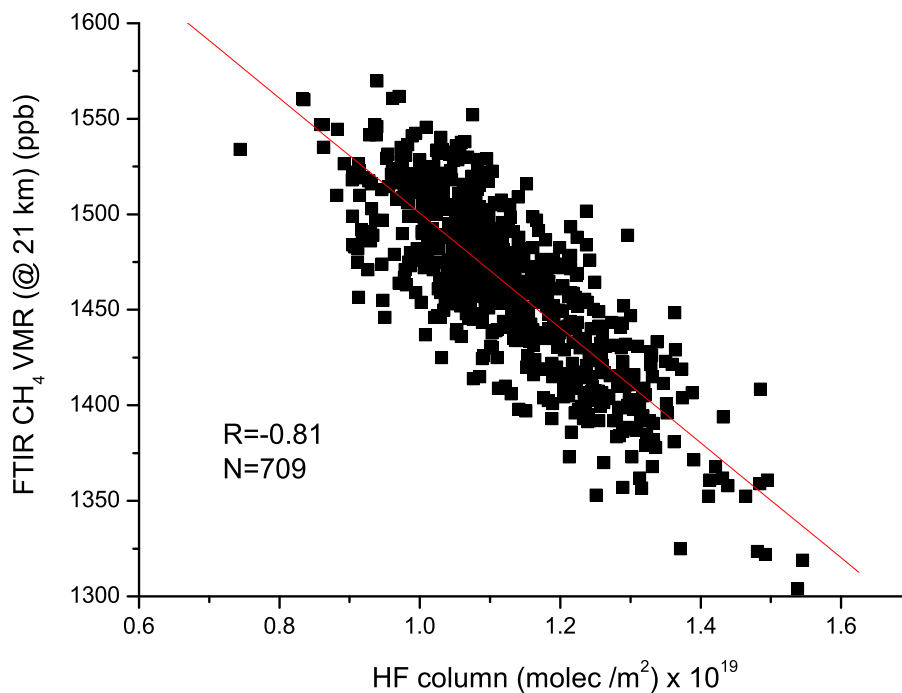
**Fig. 8.** Correlation plot of the retrieved total HF column versus $CH_4$ VMR in the UT/LS region (at 21 km). The red line shows the linear regression line.
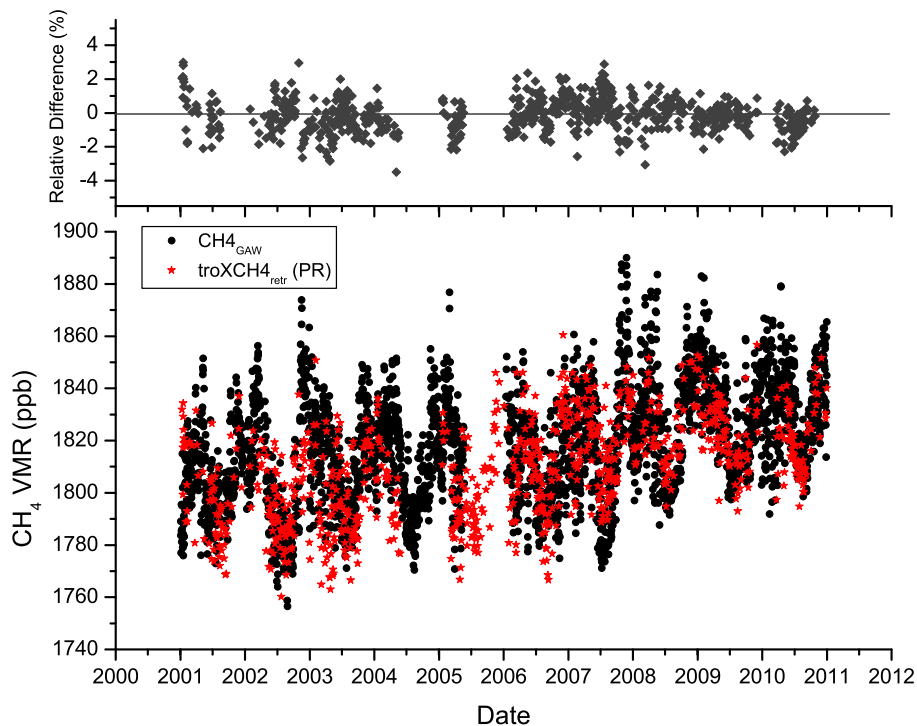
**Fig. 9.** Same as Fig. 5, but for the directly retrieved tropospheric $X$CH$_4$ (troXCH4$_{retr}$, red stars) from the profile retrieval.
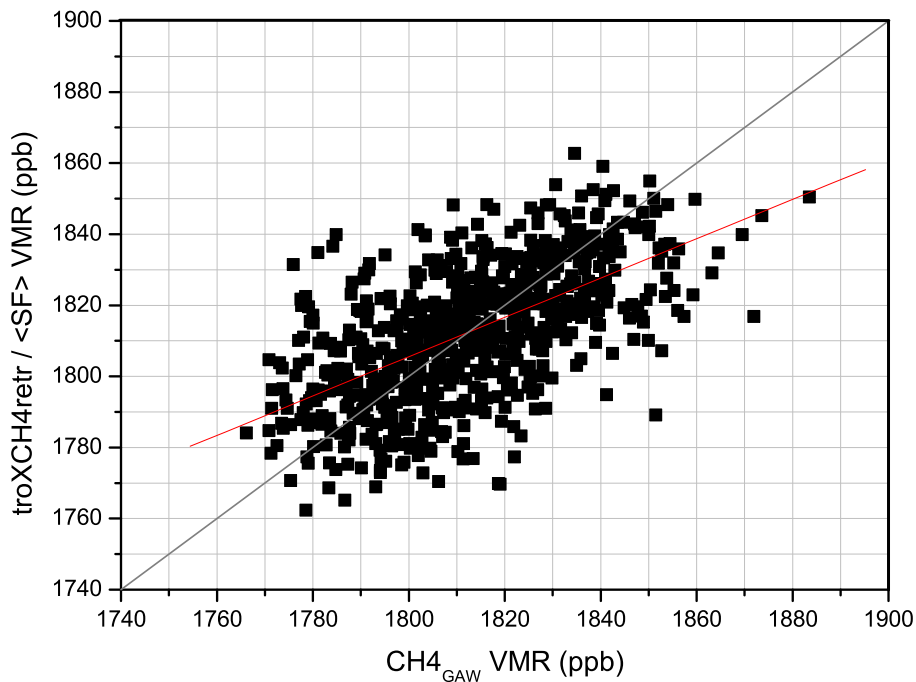
**Fig. 10.** CH$_{4_{GAW}}$ in-situ versus troXCH4$_{retr}$/<SF> correlation plot. <SF> is the mean scaling factor between both quantities. The red line shows the linear regression line while the grey one shows the diagonal as a reference.
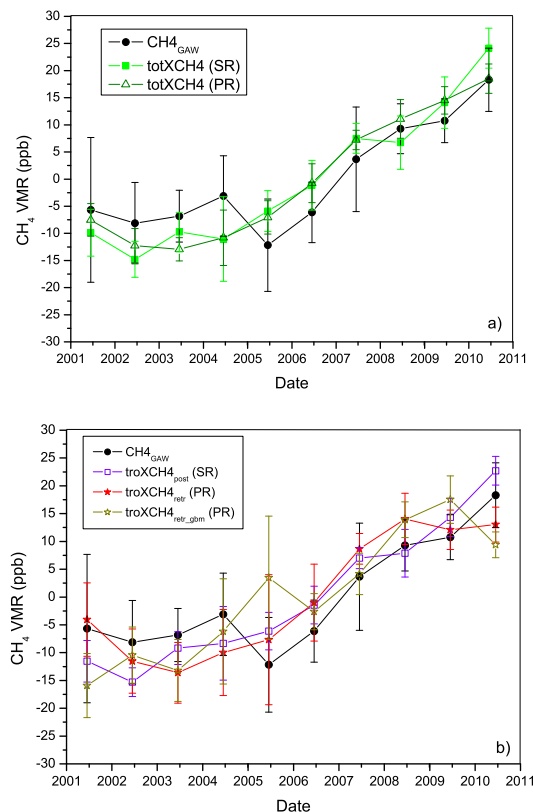
**Fig. 11.** Annual mean for the $CH4_{GAW}$ in-situ (black dots) and the different FTIR products considering coincident data and centered at zero. **(a)** total $XCH_4$ products: green squares for totXCH4 from SR, and green dark open triangles for totXCH4 from PR; **(b)** tropospheric $XCH_4$ products: violet open squares for troXCH4$_{post}$, red stars for troXCH4$_{retr}$, and open dark yellow stars for troXCH4$_{retr\_gbm}$. The error bars correspond to the standard error of the mean [$2 \times$ std/sqrt($N$)].
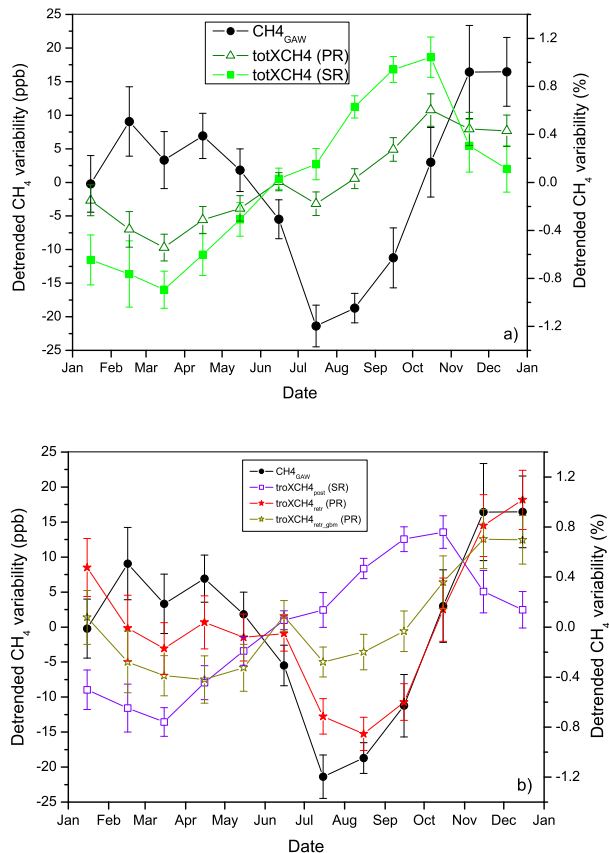
**Fig. 12.** The multi-annual mean annual cycles derived for data of the 2001–2010 period for the different $CH_{4_{GAW}}$ (black dots) and the different FTIR products: **(a)** total $XCH_4$ products; green squares for SR and green dark open triangles for PR; **(b)** tropospheric $XCH_4$ products: violet open squares for troXCH4$_{post}$, red stars for troXCH4$_{retr}$ and open dark yellow stars for troXCH4$_{retr\_gbm}$. The error bars correspond to the standard error of the mean [$2 \times std/sqrt(N)$].
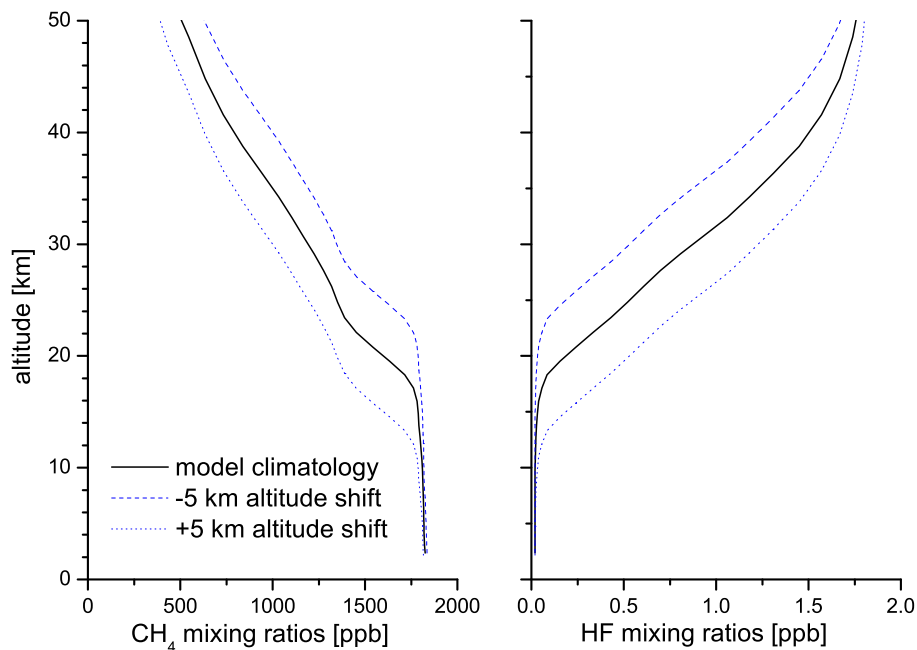
**Fig. A1.** Modeled CH$_4$ (left panel) and HF (right panel) mixing ratio profiles. Black solid lines: original model results; blue dashed and dotted lines: profiles shifted vertically by $+5$ km and $-5$ km respectively.
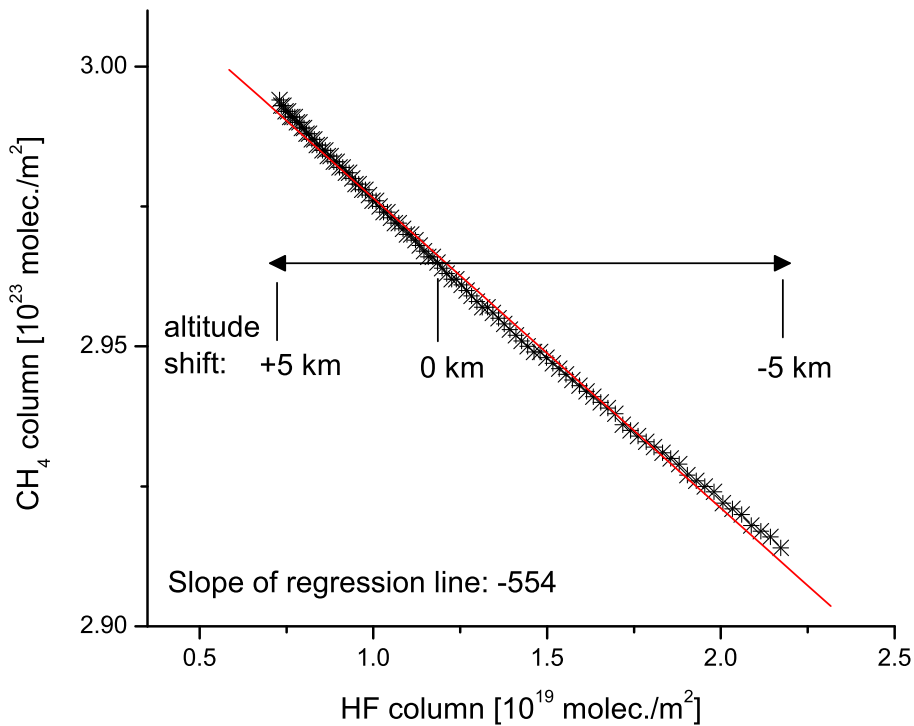
**Fig. A2.** Correlation plot between the $CH_4$ and HF total column amounts obtained for different vertical shifts of the modeled $CH_4$ and HF profiles of Fig. A1.
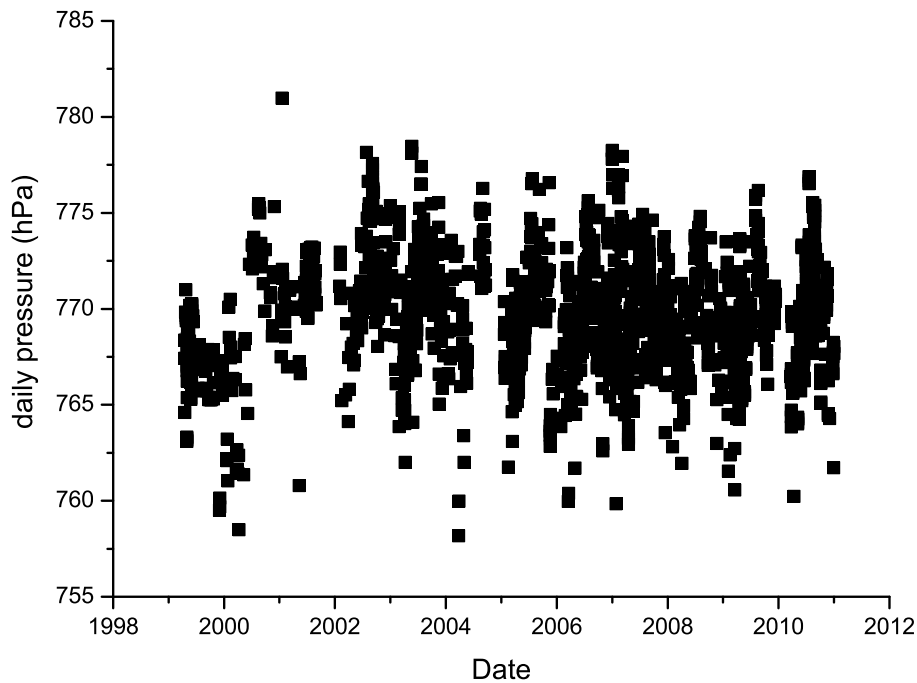
**Fig. B1.** Time series of the daily mean pressure at Izaña ground level.